

Strongly Coupled Two-scale System with Nonlinear Dispersion: Weak Solvability and Numerical Simulation

Vishnu Raveendran*, Surendra Nepal, Rainey Lyons, Michael Eden, Adrian Muntean

Department of Mathematics and Computer Science,
Karlstad University, Sweden

February 13, 2024

Abstract

We investigate a two-scale system featuring an upscaled parabolic dispersion-reaction equation intimately linked to a family of elliptic cell problems. The system is strongly coupled through a dispersion tensor, which depends on the solutions to the cell problems, and via the cell problems themselves, where the solution of the parabolic problem interacts nonlinearly with the drift term. This particular mathematical structure is motivated by a rigorously derived upscaled reaction-diffusion-convection model that describes the evolution of a population of interacting particles pushed by a large drift through an array of periodically placed obstacles (i.e., through a regular porous medium).

We prove the existence of weak solutions to our system by means of an iterative scheme, where particular care is needed to ensure the uniform positivity of the dispersion tensor. Additionally, we use finite element-based approximations for the same iteration scheme to perform multiple simulation studies. Finally, we highlight how the choice of micro-geometry (building the regular porous medium) and of the nonlinear drift coupling affects the macroscopic dispersion of particles.

Key words: Two-scale system; Nonlinear dispersion; Weak solutions; Iterative scheme; Simulation;
MSC2020: 35G55; 35A01; 35M30; 47J25; 65M60.

1 Introduction

The transport of substances through porous media typically involves a combination of drift, diffusion, and adsorption processes, all of which take place at the scale of the heterogeneous porous structure. The interplay between these physical processes and the geometry of the underlying heterogeneous structure is intricate. Only in rare circumstances can one obtain useful insight into the quantitative understanding of the effective dispersion mechanisms (responsible for an eventual macroscopic migration of substances), the overall storage capacity of a given heterogeneous medium, or the resulting turbulent diffusion and anomalous forms of dissipation; see e.g. [34] for a discussion of simple turbulent flows conveying microstructure information. However, understanding

*vishnu.raveendran@kau.se

these phenomena is crucial for a number of modern technological applications, including the design of drug delivery systems, remediation of groundwater contamination, design of efficient hydrogen storage systems, creation of polymer-based morphologies to facilitate current transport for organic solar cells; we refer the reader to [19, 27, 14] for examples of such applications.

In this work, we are primarily interested in understanding what effects are observable at a macroscopic level, i.e. in terms of the effective indicators, within the interplay between fast drift and diffusion. In other words, we are revisiting the Taylor-Aris notion of dispersion now taking place within a specific type of heterogeneous medium¹. As a first step, we are neither looking at processes related to sorption/adsorption mechanisms nor to surface chemical reactions, even though we are aware that such interface processes take place in real materials and can have an effect on the macroscopic response. We are, of course, not the first ones to look at Taylor-Aris dispersion for spatially structured domains. The majority of the previous approaches aimed to justify that the macroscopic transport mechanisms can be effectively modeled via a constant dispersion tensor which encodes both the geometric properties of the underlying microstructure (like porosity and connectivity) and the diffusivity of the solute. Such effective models for transport in porous media are usually derived via some type of scale analysis; this can be the reference elementary volume (REV) approach often utilized in the engineering community [12, 13, 47], or the more rigorous route of mathematical homogenization [4, 6, 8]. In these works, the resulting limit problem is structurally identical to a diffusion problem and the constant symmetric effective dispersion can be directly calculated via cell problems. However, in some situations, this perspective is too simplistic as the physical reality is more complicated. For instance, earlier investigations have shown that the resulting dispersion tensor may not be symmetric [11] and that it can depend (linearly or nonlinearly) on the solute concentration [43]. Such effects cannot be captured in the averaging aforementioned approaches.

To this end, we are considering a dispersion-reaction equation governing the effective solute transport and production in a porous medium where the dispersion depends nonlinearly on the solute concentration,

$$\partial_t u + \operatorname{div}(-D^*(W)\nabla u) = f \quad \text{in } (0, T) \times \Omega, \quad (1a)$$

over some macroscopic domain $\Omega \subset \mathbb{R}^2$ representing a porous medium. While Equation (1a) is macroscopic, the dispersion tensor $D^*(W)$ depends on microscopic solutions $W = (w_1, w_2)$ of cell problems over the fluid part of the porous microstructure Y via

$$\operatorname{div}_y(-D\nabla_y w_i + G_i(u)Bw_i) = \operatorname{div}_y(De_i) \quad \text{in } Y, \quad (i = 1, 2). \quad (1b)$$

Here, D denotes the solute diffusivity, B the velocity field representing the movement of the solvent, and $G_i(u)$ the drift coupling. Via the product $G_i(u)Bw_i$, the macroscopic function u nonlinearly interacts with the cell problem solution W . Without this specific interaction in the cell problems, i.e., taking the case $G_i(u) \equiv \text{const.}$, the dispersion tensor assumes the standard form of linear dispersion, see [6]. Moreover, the case $G_i(u) \equiv 0$ corresponds to pure diffusion [2].

The structure of our model is motivated by the homogenization limit $\varepsilon \rightarrow 0$ of a fast drift problem of the form

$$\partial_t u^\varepsilon + \operatorname{div}(-D^\varepsilon \nabla u^\varepsilon + \frac{1}{\varepsilon} B^\varepsilon P(u^\varepsilon)) = f^\varepsilon, \quad (2)$$

¹G. I. Taylor tells in his 1954 paper [45] that shear flow smears out the concentration distribution, enhancing the rate at which it spreads in the direction of the flow. R. Aris confirms that the effect takes place at large Peclet numbers (see [9]).

where $0 < \varepsilon \ll 1$ is a small scale parameter representative of the porous geometry which is assumed to be periodic; we refer to [42] for more details regarding this limiting process. The ε -dependent problem with nonlinear fast drift given by Equation (2) is associated with a hydrodynamic limit of a *totally asymmetric simple exclusion process* (TASEP) which describes a population of interacting particles crossing a domain with obstacles [18, 17, 40]. In this scenario, the nonlinearity takes the form $P(r) := r(1 - r)$ which corresponds to $G_i(r) = 1 - 2r$ in Equation (1b) (see [42]). Since nonlinear interactions in the diffusion/dispersion part come up quite often in upscaled models, e.g., [33, 5, 25, 15], we study the case where the terms $G_i(u)$ are general functions which satisfy certain assumptions presented later. It is worth noting that our scientific questions are very much in the spirit of [23], where the authors ask: what is the macroscopic response of

$$\partial_t u^\varepsilon + \operatorname{div}(-\eta \nabla u^\varepsilon + u^\varepsilon V^\varepsilon) = f^\varepsilon, \quad (3)$$

where $\eta > 0$ and V^ε is some large random field? In other words, what precisely is the term $\langle uV \rangle$ in the corresponding upscaled equation

$$\partial_t \langle u \rangle + \operatorname{div}(-\eta \nabla \langle u \rangle + \langle uV \rangle) = \langle f \rangle, \quad (4)$$

where $\langle \cdot \rangle$ denotes some suitable average, and how can this be computed numerically. Comparing (3) and (4) with (2) and (1a), we see that the vector field V^ε is in our setting what the TASEP requires, and hence, the meaning of $\langle uV \rangle$ is for us precisely $-D^*(W)\nabla u$.

System (1) is an example of a two-scale system, where we refer to the dispersion equation (1a) as the macroscopic equation and the cell problems (1b) as the microscopic equations. Such systems are also referred to as distributed-microstructure models, terminology introduced by R. E. Showalter in [44]. The presence of nonlinear coupling in the dispersion tensor has been previously studied. For instance, in [20], the authors looked at the nonlinear effect of colloids deposition on diffusion in porous media and established local-in-time existence (see also [35, 37]). In the same context, in [46] a similar model was analyzed via homogenization techniques. Additionally, a related homogenized model for reactive flows in porous media was derived in [5].

The simulation of such scale separated problems often come with unique computational challenges. For instance, the nonlinear drift coupling in the cell problems requires solving Equation (1b) many times. Well-established numerical techniques capable of handling such multiscale features are reported in [3, 24, 1, 16]. Some of the closer works that explore the simulation of two-scale systems similar to ours are [29, 38, 37]. In [29], the authors address a two-scale coupled problem where the coupling is via the reaction rate of macroscopic equation. On the other hand, authors in [38] study and simulate a two-scale system for a phase-field model for precipitation and dissolution in porous media via an iterative scheme and, in [37], clogging of a porous medium via aggregation of colloidal particles was explored.

This paper is structured as follows: In Section 2, we present the mathematical model of interest, the geometric setup, as well as the assumptions on coefficients and data needed for the mathematical analysis. This is followed by Section 3 where the main result, namely the existence of solutions (Theorem 2), is proven via an iteration scheme. In Section 4, we use this iteration scheme to numerically simulate different scenarios, showcasing that the proposed two-scale model is able to capture interesting effects at both the microscopic and macroscopic scale. The results reported in this section are only preliminary, as the numerical analysis and further numerical exploration of our system are postponed for follow-up work. Finally in Section 5, we conclude our work with a short summary of the findings and with a discussion of possible future investigations.

2 Setting of the problem

Let $T > 0$ represent the time horizon. We denote by $\Omega \subset \mathbb{R}^2$ a non-empty open bounded domain with $C^{2+\alpha}$ boundary, $\partial\Omega$, for some $0 < \alpha < 1$, and by $Y_0 \subset (0,1)^2$ a compact set with positive measure and Lipschitz boundary such that the microscopic domain $Y := (0,1)^2 \setminus Y_0$ is connected. We let $t \in (0, T)$ represent the time variable, $x \in \Omega$ the macroscopic space variable, $y \in Y$ the microscopic space variable, $\Gamma_N = \partial Y_0$, and n_y the outward unit normal vector across the interface ∂Y . With the sets Ω and Y at hand, we can build a two-scale geometry. For a schematic representation of such a geometry, see Figure 1. We take e_i , $i = 1, 2$, to denote the standard unit basis vectors in \mathbb{R}^2 .

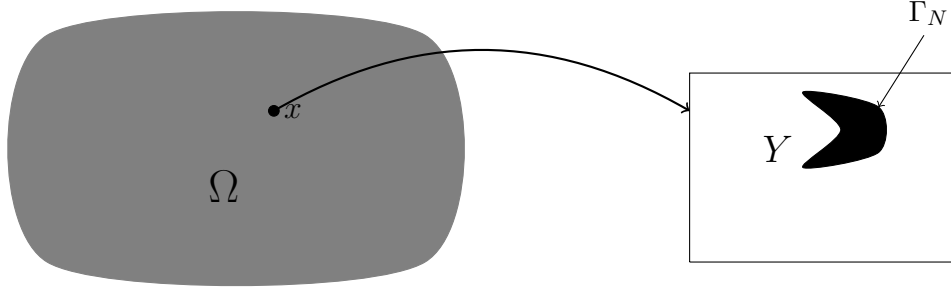


Figure 1: Typical two-scale geometry: schematic representation of the macroscopic domain Ω and of the microscopic domain Y with internal boundary Γ_N .

We study the following nonlinear two-scale system:

Problem $P(\Omega)$

Find the unknown functions u and $W := (w_1, w_2)$ satisfying

$$\partial_t u + \operatorname{div}(-D^*(W)\nabla u) = f \quad \text{in } (0, T) \times \Omega, \quad (5a)$$

$$u = 0 \quad \text{on } (0, T) \times \partial\Omega, \quad (5b)$$

$$u(0) = g \quad \text{in } \bar{\Omega}, \quad (5c)$$

$$\operatorname{div}_y(-D\nabla_y w_i + G_i(u)Bw_i) = \operatorname{div}_y(De_i) \quad \text{in } Y, \quad (5d)$$

$$(-D\nabla_y w_i + BG_i(u)w_i) \cdot n_y = (De_i) \cdot n_y \quad \text{on } \Gamma_N, \quad (5e)$$

$$w_i \text{ is } Y\text{-periodic.} \quad (5f)$$

Relating back to our motivation discussed in Section 1 (cf. also [42, 18]), u represents the particle concentration on macroscopic porous domain Ω , while W , the solution to cell problems, relays the microscopic information, including the shape of the domain, drift, and diffusion, to the macroscopic scale via the dispersion tensor, $D^*(W)$, given by

$$D^*(W) := \frac{1}{|Y|} \int_Y D(y) \left(I + \begin{bmatrix} \frac{\partial w_1}{\partial y_1} & \frac{\partial w_2}{\partial y_1} \\ \frac{\partial w_1}{\partial y_2} & \frac{\partial w_2}{\partial y_2} \end{bmatrix} \right) dy \quad (6)$$

where I is the 2×2 identity matrix and $|Y|$ is the Lebesgue measure of the set Y . The periodic boundary condition (5f) and the Neumann influx boundary condition (5e) are common in effective models derived by homogenization (see [31]).

We assume the reaction rate $f : (0, T) \times \Omega \rightarrow \mathbb{R}$, the initial condition $g : \Omega \rightarrow \mathbb{R}$, the microscopic diffusion matrix $D : Y \rightarrow \mathbb{R}^{2 \times 2}$, the microscopic velocity field $B : Y \rightarrow \mathbb{R}^2$, and the nonlinear functions $G_1, G_2 : \mathbb{R} \rightarrow \mathbb{R}$ are given and satisfy additional assumptions discussed later. Note that, to calculate the macroscopic equation and dispersion tensor, we need to, at each point $(t, x) \in (0, T) \times \Omega$, solve the microscopic problem in Y .

To discuss the concept of weak solution to Problem $P(\Omega)$, we introduce the following functional spaces:

$$\begin{aligned} H_{\#}^1(Y) &:= \{v \in H^1(Y) : v \text{ is } Y\text{-periodic}\}, \\ \mathcal{U} &:= \{v \in L^2((0, T); H_0^1(\Omega)) : \partial_t v \in L^2((0, T); H^{-1}(\Omega))\}, \\ \text{and } \mathcal{W} &:= \left\{ v \in H_{\#}^1(Y) : \int_Y v(y) \, dy = 0 \right\}, \end{aligned}$$

where $H_{\#}^1(Y)$ is equipped with the standard $H^1(Y)$ norm. We denote by $\langle \cdot, \cdot \rangle$ the duality pairing between $H^{-1}(\Omega)$ and $H_0^1(\Omega)$. Finally, we define the weak solution of Problem $P(\Omega)$ in the following sense:

Definition 2.1. *We say that (u, W) is a weak solution to Problem $P(\Omega)$ if $u \in \mathcal{U}$ with $u(0, \cdot) = g$ and, for almost every $(t, x) \in (0, T) \times \Omega$, $w_i \in \mathcal{W}$ and the following integral equations are satisfied:*

$$\langle \partial_t u, \phi \rangle + \int_{\Omega} D^*(W) \nabla u \cdot \nabla \phi \, dx = \int_{\Omega} f \phi \, dx, \quad (7a)$$

$$\int_Y (D \nabla_y w_i - G_i(u(t, x)) B w_i) \cdot \nabla_y \psi \, dy = \int_Y \operatorname{div}_y (D e_i) \psi \, dy - \int_{\Gamma_N} D e_i \cdot n_y \psi \, d\sigma, \quad (7b)$$

for all $(\phi, \psi) \in H^1(\Omega) \times H_{\#}^1(Y)$ and $i \in \{1, 2\}$.

Assumptions. From now on C denotes a positive real number, possibly changing its value from line to line. We consider the following restrictions on data and model parameters:

(A1) The microscopic diffusion matrix satisfies $D \in (H_{\#}^1(Y) \cap L^{\infty}(Y))^{2 \times 2}$ and there exists $\theta > 0$ such that

$$\theta |\eta|^2 \leq D \eta \cdot \eta \quad \text{for all } \eta \in \mathbb{R}^2 \text{ and almost all } y \in Y;$$

(A2) $G_1, G_2 : \mathbb{R} \rightarrow \mathbb{R}$ are locally Lipschitz functions, i.e., Lipschitz on compact sets;

(A3) The microscopic drift velocity $B \in (H_{\#}^1(Y) \cap L^{\infty}(Y))^2$ satisfies

$$\begin{cases} \operatorname{div}_y B = 0 & \text{in } Y, \\ B \cdot n_y = 0 & \text{on } \Gamma_N; \end{cases}$$

(A4) The reaction rate satisfies $f \in C^{\alpha, \frac{\alpha}{2}}((0, T) \times \Omega)$ and the initial condition $g \in C^{2+\alpha}(\Omega)$, for some $0 < \alpha < 1$.

Assumptions (A1)-(A4) may seem technical but can be satisfied by many physically relevant functions. For example, Assumption (A2) can be satisfied by taking B to be the solution to an incompressible Stokes problem with no penetration into the obstacle and periodic boundary conditions across $\partial Y \setminus \Gamma_N$. This is also the approach we have taken in our simulations, see Section 4.

We remark that in Problem $P(\Omega)$ we can also have nonhomogeneous Dirichlet boundary conditions $u = h$ on $\partial\Omega$ for some given $h \in H^{\frac{1}{2}}(\Omega)$. This regularity allows us to extend h to $\tilde{h} \in H^1(\Omega)$ and transform the original problem into

$$\begin{aligned} \partial_t \tilde{u} + \operatorname{div}(-D^*(W)\nabla_x \tilde{u}) &= \tilde{f}(W) && \text{in } (0, T) \times \Omega, \\ \tilde{u} &= 0 && \text{on } (0, T) \times \partial\Omega, \\ \tilde{u}(0) &= \tilde{g} && \text{in } \bar{\Omega}, \\ \operatorname{div}_y \left(-D\nabla_y w_i + G_i(\tilde{u} + \tilde{h})Bw_i \right) &= \operatorname{div}_y(De_i) && \text{in } Y, \\ \left(-D\nabla_y w_i + BG_i(\tilde{u} + \tilde{h})w_i \right) \cdot n_y &= (De_i) \cdot n_y && \text{on } \Gamma_N, \\ w_i &\text{ is } Y\text{-periodic,} \end{aligned}$$

where $\tilde{u} := u - \tilde{h}$, $\tilde{f}(W) := f - \operatorname{div}(D^*(W)\nabla \tilde{h})$ and $\tilde{g} := g - \tilde{h}$.

3 Weak solvability of Problem $P(\Omega)$

In this section, we prove the existence of solutions to Problem $P(\Omega)$ in the sense of Definition 2.1. There are two main difficulties in the analysis of the involved equations: (i) the nonlinear coupling in the drift, and (ii) the positivity of the dispersion tensor.

The main strategy of our proof follows four distinct steps:

- Step 1: We construct a two-scale iterative scheme based on Problem $P(\Omega)$. This scheme is constructed by decoupling $P(\Omega)$ into a family of linear problems, which we refer to as $P^k(\Omega)$, $k \in \mathbb{N}$. The notion of weak solutions (u^k, W^k) to Problem $P^k(\Omega)$ is given in Definition 3.1.
- Step 2: We construct an auxiliary problem similar to (5d)–(5f) and show it is well-posed in Lemma 1. This helps us to understand the coupling between $G_i(u^k)$ and W^k . We then show in Lemma 3 that the dispersion tensor is bounded and positive definite, uniformly with respect to the index k .
- Step 3: With Lemma 1 and Lemma 3, we show that for each k the problems $P^k(\Omega)$ are well-posed, their solutions satisfy k -independent energy estimates, and are also uniformly bounded; see both Theorem 1 and Lemma 4.
- Step 4: Finally, we prove our main result (Theorem 2) – the solution to the iterative scheme converges in a suitable sense to a solution to Problem $P(\Omega)$.

3.1 Iterative scheme

We begin by introducing the iterative scheme and its corresponding weak formulation. We set $u^0 = g$, and, for any $k \in \mathbb{N} \cup \{0\}$, we denote as u^{k+1} , w_1^k , and w_2^k the solutions to the following decoupled system:

Diffusion-drift problem

$$\operatorname{div}_y \left(-D \nabla_y w_i^k + G_i(u^k) B w_i^k \right) = \operatorname{div}_y (D e_i) \quad \text{in } Y, \quad (8a)$$

$$\left(-D \nabla_y w_i^k + B G_i(u^k) w_i^k \right) \cdot n_y = (D e_i) \cdot n_y \quad \text{on } \Gamma_N, \quad (8b)$$

$$w_i^k \text{ is } Y\text{-periodic}, \quad i \in \{1, 2\} \quad (8c)$$

Reaction-dispersion problem

$$\partial_t u^{k+1} + \operatorname{div}(-D^*(W^k) \nabla_x u^{k+1}) = f \quad \text{in } (0, T) \times \Omega, \quad (8d)$$

$$u^{k+1}(0) = g \quad \text{in } \bar{\Omega}, \quad (8e)$$

$$u^{k+1} = 0 \quad \text{on } (0, T) \times \partial\Omega, \quad (8f)$$

where the dispersion tensor $D^*(W^k)$ is given by

Effective dispersion tensor

$$D^*(W^k) := \frac{1}{|Y|} \int_Y D(y) \left(I + \begin{bmatrix} \frac{\partial w_1^k}{\partial y_1} & \frac{\partial w_2^k}{\partial y_1} \\ \frac{\partial w_1^k}{\partial y_2} & \frac{\partial w_2^k}{\partial y_2} \end{bmatrix} \right) dy. \quad (8g)$$

We refer to the iterative scheme (8a)–(8f) together with (8g), as Problem $P^k(\Omega)$. We define the concept of weak solutions to Problem $P^k(\Omega)$ in a similar manner as for the Problem $P(\Omega)$ (see Definition 2.1).

Definition 3.1. *Given $u^k \in \mathcal{U}$, we say that (u^{k+1}, W^k) is a weak solution to Problem $P^k(\Omega)$ if $u^{k+1} \in \mathcal{U}$ with $u^{k+1}(0, \cdot) = g$ and, for almost every $(t, x) \in (0, T) \times \Omega$, $w_i^k \in \mathcal{W}$ and the following integral equations are satisfied:*

$$\langle \partial_t u^{k+1}, \phi \rangle + \int_{\Omega} D^*(W^k) \nabla u^{k+1} \cdot \nabla \phi dx = \int_{\Omega} f \phi dx \quad (9a)$$

$$\int_Y \left(D \nabla_y w_i^k - G_i(u^k(t, x)) B w_i^k \right) \cdot \nabla_y \psi dy = \int_Y \operatorname{div}_y (D e_i) \psi dy - \int_{\Gamma_N} D e_i \cdot n_y \psi d\sigma, \quad (9b)$$

for all $(\phi, \psi) \in H^1(\Omega) \times H_{\#}^1(Y)$ and $i \in \{1, 2\}$.

3.2 Existence results for the Problem $P^k(\Omega)$

In this section, we study the well-posedness of the iterative scheme (8a)–(8g). To analyze the scheme, we first focus on the elliptic equation (8a)–(8c) by constructing an auxiliary problem similar to (5d)–(5f). We show this auxiliary problem is well-posed, prove energy estimates, and establish the regularity of weak solutions. Then with the help of Lemma 3, which establishes the uniform positive definite property and boundedness of $D^*(W^k)$, we show our iterative scheme Problem $P^k(\Omega)$ is well-posed.

Lemma 1. *Let $p \in \mathbb{R}$. Consider the following auxiliary problem: Find $W(p, \cdot) = (w_1(p, \cdot), w_2(p, \cdot)) \in \mathcal{W}^2$ satisfying*

$$\operatorname{div}_y (-D \nabla_y w_i + p B w_i) = \operatorname{div}_y (D e_i) \quad \text{in } Y, \quad (10a)$$

$$(-D\nabla_y w_i + pBw_i) \cdot n_y = (De_i) \cdot n_y \quad \text{on } \Gamma_N, \quad (10b)$$

$$w_i \text{ is } Y\text{-periodic}, \quad (10c)$$

where $i \in \{1, 2\}$. Assume (A1)–(A2) holds, then

(i) there exists a unique weak solution $w_i(p, \cdot) \in \mathcal{W}$ to the problem (10a)–(10c),

(ii) there exists a constant $C > 0$ independent of p such that

$$\|\nabla_y w_i(p, \cdot)\|_{L^2(Y)} \leq C, \quad (11)$$

(iii) there exists a constant $C > 0$ such that, for all $p_1, p_2 \in \mathbb{R}$,

$$\int_Y |\nabla_y (w_i(p_1, y) - w_i(p_2, y))|^2 dy \leq C|p_1 - p_2|^2. \quad (12)$$

Proof. (i) We begin by stating the weak form of (10a)–(10c):

$$\int_Y (D\nabla_y w_i - pBw_i) \cdot \nabla_y \psi dy = \int_Y \operatorname{div}_y (De_i) \psi dy - \int_{\Gamma_N} De_i \cdot n_y \psi d\sigma \quad (13)$$

for all $\psi \in H_{\#}^1(Y)$ and $i \in \{1, 2\}$. From (A1), we have

$$\int_Y \operatorname{div}_y (D(y)e_i) dy = \int_{\Gamma_N} (D(y)e_i) \cdot n_y d\sigma. \quad (14)$$

Using identity (14) together with standard arguments involving the classical Fredholm alternative, we have the existence and uniqueness of $w_1(p, \cdot)$ and $w_2(p, \cdot)$ in the sense of (13) (for details we refer the reader [4, Section 4]).

(ii) First, using integration by parts, we have the following equation:

$$\begin{aligned} \int_Y pBw_i \cdot \nabla_y w_i dy &= \frac{p}{2} \int_Y B\nabla_y (w_i^2) dy \\ &= \frac{p}{2} \int_Y w_i^2 \operatorname{div}_y B dy + \frac{p}{2} \int_{\partial Y \setminus \Gamma_N} B \cdot n_y w_i^2 d\sigma \\ &\quad + \frac{p}{2} \int_{\Gamma_N} B \cdot n_y w_i^2 d\sigma. \end{aligned} \quad (15)$$

By (A2), we have that $\int_Y w_i^2 \operatorname{div}_y B dy = 0$ and $\int_{\Gamma_N} B \cdot n_y w_i^2 d\sigma = 0$. Additionally, by the periodicity of w_i and B , we have $\int_{\partial Y \setminus \Gamma_N} B \cdot n_y w_i^2 d\sigma = 0$, and so we obtain

$$\int_Y pBw_i \cdot \nabla_y w_i dy = 0. \quad (16)$$

Now, taking the test function $\psi = w_i$ in the weak formulation (13) and making use of (16), we obtain

$$\int_Y D\nabla_y w_i \cdot \nabla_y w_i dy = \int_Y \operatorname{div}_y (De_i) w_i dy - \int_{\Gamma_N} (De_i) \cdot n_y w_i d\sigma. \quad (17)$$

Making use of (A1) and integration by parts, we see that

$$\theta \int_Y |\nabla_y w_i|^2 dy \leq \int_Y |(De_i) \nabla_y w_i| dy. \quad (18)$$

Young's inequality applied to the right-hand side of (18) together with (A1), yields (11).

(iii) Let

$$\overline{w_i} := w_i(p_1, y) - w_i(p_2, y) \text{ and } \overline{p} := p_1 - p_2$$

and consider the weak formulations (13) with $p = p_1, p_2$. We take the test function $\psi = \overline{w_i}$ in both weak forms and subtract the equations to arrive at

$$\int_Y (D(y) \nabla_y \overline{w_i} - B(y)(p_1 w_i(p_1, y) - p_2 w_i(p_2, y))) \cdot \nabla_y \overline{w_i} dy = 0. \quad (19)$$

Adding and subtracting the term $\int_Y B(y) p_2 w_i(p_1, y) dy$ to (19) and making use of assumption (A1), we obtain

$$\theta \int_Y |\nabla_y \overline{w_i}|^2 dy \leq \int_Y B(y) (\overline{p} w_i(p_1, y) + p_2 \overline{w_i}) \cdot \nabla_y \overline{w_i} dy. \quad (20)$$

Since w_1 and w_2 are periodic, $\overline{w_i}$ is periodic as well. Therefore, we may follow similar arguments which lead to (16) to obtain

$$\int_Y B(y) p_2 \overline{w_i} \cdot \nabla_y \overline{w_i} dy = 0. \quad (21)$$

Returning to (20), using Young's inequality, we have

$$\begin{aligned} \theta \int_Y |\nabla_y \overline{w_i}|^2 dy &\leq \int_Y B(y) \overline{p} w_i(p_1, y) \cdot \nabla_y \overline{w_i} dy \leq C \overline{p} \int_Y |w_i(p_1, y)| |\nabla_y \overline{w_i}| \\ &\leq \frac{1}{2\theta} |\overline{p}|^2 \|w_i(p_1)\|_{L^2(Y)}^2 + \frac{\theta}{2} \int_Y |\nabla_y \overline{w_i}|^2 dy. \end{aligned} \quad (22)$$

Then, with (11), we arrive at

$$\int_Y |\nabla_y \overline{w_i}|^2 dy \leq C |\overline{p}|^2. \quad (23)$$

□

To study the weak solvability of (8d)–(8f), we first show that the dispersion tensor (8g) is both uniformly positive definite and uniformly bounded. To this end, for any $p \in \mathbb{R}$, we define $\overline{D}(p) \in \mathbb{R}^{2 \times 2}$ by

$$[\overline{D}(p)]_{i,j} := \frac{1}{|Y|} \int_Y D(y) (e_j + \nabla_y w_j(p, y)) \cdot e_i dy, \quad (24)$$

where $i, j \in \{1, 2\}$ and $w_j(p, y)$ is the weak solution to (10a)–(10c). We begin by showing that the matrix $\overline{D}(p)$ is Lipschitz continuous with respect to p .

Lemma 2. *Assume (A1)–(A2) hold. There exists a constant $C > 0$, independent of p and q , such that*

$$|[\overline{D}(p)]_{i,j} - [\overline{D}(q)]_{i,j}| \leq C |p - q|.$$

Proof. From definition (24), assumption (A1), and Lemma 1 (iii), we have

$$\begin{aligned} |[\overline{D}(p)]_{i,j} - [\overline{D}(q)]_{i,j}| &\leq C \int_Y |D(y)| |\nabla_y(w_i(p, y) - w_i(q, y))| \, dy \\ &\leq C \left(\int_Y |\nabla_y(w_i(p, y) - w_i(q, y))|^2 \, dy \right)^{\frac{1}{2}} \\ &\leq C|p - q|. \end{aligned} \tag{25}$$

□

We now show that the dispersion tensor is both uniformly bounded and uniformly positive definite.

Lemma 3. *Assume (A1)–(A2) hold and let $M > 0$. For $p = (p_1, p_2) \in [-M, M]^2$, let $W_p := (w_1(p_1, \cdot), w_2(p_2, \cdot))$ be the corresponding solutions of the auxiliary problem (10a)–(10c). Then the macroscopic dispersion tensor $D^*(W_p)$ satisfies the following properties:*

(i) *There exists $\theta_M > 0$ independent of p such that*

$$\theta_M |\eta|^2 \leq D^*(W_p) \eta \cdot \eta \quad \text{for all } \eta \in \mathbb{R}^2; \tag{26}$$

(ii) *There exist a constant $C > 0$ independent of p such that*

$$|[D^*(W_p)]_{i,j}| \leq C, \quad (i, j \in \{1, 2\}). \tag{27}$$

Proof. (i) From the definition of $\overline{D}(\cdot)$ (24) and the definition of $D^*(\cdot)$ (6), we have

$$[D^*(W_p)]_{i,j} = [\overline{D}(p_i)]_{i,j}, \tag{28}$$

and hence,

$$[D^*(W_p)]_{i,j} = \frac{1}{|Y|} \int_Y D(y) (e_j + \nabla_y w_j(p_i, y)) \cdot e_i \, dy. \tag{29}$$

We consider the weak formulation for the problem (10a)–(10c) (i.e., Equation (13)) for index j , where we choose the test function $\psi = w_i$ and divide by $|Y|$:

$$\frac{1}{|Y|} \int_Y (D \nabla_y w_j - p_j B w_j) \cdot \nabla_y w_i \, dy = \frac{1}{|Y|} \int_Y \operatorname{div}_y (D e_j) w_i \, dy - \frac{1}{|Y|} \int_{\Gamma_N} (D e_j) \cdot n_y w_i \, d\sigma. \tag{30}$$

Using integration by parts on $\int_Y \operatorname{div}_y (D e_j) w_i \, dy$ and noting the periodicity of $D(\cdot)$ and $w_i(\cdot)$, we arrive at

$$\frac{1}{|Y|} \int_Y (D \nabla_y w_j - p_j B w_j + D e_j) \cdot \nabla_y w_i \, dy = 0. \tag{31}$$

Adding (31) to (29), we see that

$$[D^*(W_p)]_{i,j} = [A(p)]_{i,j} + [J(p)]_{i,j}, \tag{32}$$

where

$$[A(p)]_{i,j} := \frac{1}{|Y|} \int_Y D(e_j + \nabla_y w_j) \cdot (e_i + \nabla_y w_i) \, dy, \tag{33}$$

$$\text{and } [J(p)]_{i,j} := -\frac{1}{|Y|} \int_Y p_j B w_j \cdot \nabla_y w_i \, dy. \quad (34)$$

Using (A2) and integration by parts on $\int_Y p_j B w_j \cdot \nabla_y w_i \, dy$, we obtain

$$\begin{aligned} -[J(p)]_{i,j} &= -\frac{p_j}{|Y|} \int_Y \nabla_y (B w_j) w_i \, dy + \frac{p_j}{|Y|} \int_{\partial Y} B \cdot n_y w_i w_j \, d\sigma \\ &= -\frac{1}{|Y|} \int_Y p_j B w_i \cdot \nabla_y w_j \, dy \\ &= [J(p)]_{j,i}. \end{aligned} \quad (35)$$

Combining (33) and (35) shows that $A(p)$ and $J(p)$ are the symmetric and skew-symmetric parts of $D^*(W_p)$. Since $J(p)$ is a 2×2 skew-symmetric matrix, we have

$$J(p)\eta \cdot \eta = 0 \quad \text{for all } \eta \in \mathbb{R}^2. \quad (36)$$

So, to prove (26) it is enough to establish that $A(p)$ is in fact positive definite. Since $A(p)$ is symmetric, using the structure (33) we have for all $\eta = (\eta_1, \eta_2) \in \mathbb{R}^2$,

$$\begin{aligned} A(p)\eta \cdot \eta &= \eta_1^2 \frac{1}{|Y|} \int_Y D(e_1 + \nabla_y w_1) \cdot (e_1 + \nabla_y w_1) \, dy \\ &\quad + 2\eta_1 \eta_2 \frac{1}{|Y|} \int_Y D(e_1 + \nabla_y w_1) \cdot (e_2 + \nabla_y w_2) \, dy \\ &\quad + \eta_2^2 \frac{1}{|Y|} \int_Y D(e_2 + \nabla_y w_2) \cdot (e_2 + \nabla_y w_2) \, dy. \end{aligned}$$

Distributing η_1 and η_2 inside the integrals, we get

$$\begin{aligned} A(p)\eta \cdot \eta &= \frac{1}{|Y|} \int_Y D\left(\begin{bmatrix} \eta_1 \\ 0 \end{bmatrix} + \eta_1 \nabla_y w_1\right) \cdot \left(\begin{bmatrix} \eta_1 \\ 0 \end{bmatrix} + \eta_1 \nabla_y w_1\right) \, dy \\ &\quad + 2\frac{1}{|Y|} \int_Y D\left(\begin{bmatrix} \eta_1 \\ 0 \end{bmatrix} + \eta_1 \nabla_y w_1\right) \cdot \left(\begin{bmatrix} 0 \\ \eta_2 \end{bmatrix} + \eta_2 \nabla_y w_2\right) \, dy \\ &\quad + \frac{1}{|Y|} \int_Y D\left(\begin{bmatrix} 0 \\ \eta_2 \end{bmatrix} + \eta_2 \nabla_y w_2\right) \cdot \left(\begin{bmatrix} 0 \\ \eta_2 \end{bmatrix} + \eta_2 \nabla_y w_2\right) \, dy. \end{aligned} \quad (37)$$

Rearranging the right side of the identity (37) and using (A1) yields

$$\begin{aligned} A(p)\eta \cdot \eta &= \frac{1}{|Y|} \int_Y D\left(\begin{bmatrix} \eta_1 \\ \eta_2 \end{bmatrix} + \sum_{i=1}^2 \eta_i \nabla_y w_i\right) \cdot \left(\begin{bmatrix} \eta_1 \\ \eta_2 \end{bmatrix} + \sum_{i=1}^2 \eta_i \nabla_y w_i\right) \, dy \\ &\geq \theta \frac{1}{|Y|} \int_Y |\eta + \sum_{i=1}^2 \eta_i \nabla_y w_i|^2 \, dy \\ &\geq 0. \end{aligned} \quad (38)$$

If $A(p)\eta \cdot \eta = 0$ for some $\eta \in \mathbb{R}^2$, then we have

$$|\eta + \sum_{i=1}^2 \eta_i \nabla_y w_i|^2 = 0 \quad \text{for almost every } y \in Y.$$

Consequently, this yields

$$\sum_{i=1}^2 \eta_i w_i = C - \eta \cdot y, \quad (39)$$

for some constant C . Since the w_i are periodic, identity (39) is only possible for $\eta = 0$. Hence, $A(p)\eta \cdot \eta = 0$ only for $\eta = 0$. Therefore, combining this with (36), we get

$$D^*(W_p)\eta \cdot \eta > 0. \quad (40)$$

for all $p \in [-M, M]^2$ and all $\eta \neq 0$. Define the function $F : [-M, M]^2 \times \partial B(0, 1) \rightarrow \mathbb{R}$ as

$$F(p, \xi) := D^*(W_p)\xi \cdot \xi \text{ for all } \xi \in \partial B(0, 1).$$

We have from Lemma 2 that the function $p_i \mapsto \bar{D}(p_i)$ is continuous. Using the definition (28), we see that the function $p \mapsto D^*(W_p)$ is also continuous. Therefore, F is continuous and $F(p, \xi) > 0$ over the compact set $([-M, M]^2 \times \partial B(0, 1))$. Hence, there exist a $\theta_M > 0$ such that

$$F(p, \xi) > \theta_M$$

for all $(p, \xi) \in ([-M, M]^2 \times \partial B(0, 1))$. So, for any $\eta \neq 0$ we have

$$\begin{aligned} D^*(W_p) \frac{\eta}{|\eta|} \cdot \frac{\eta}{|\eta|} &> \theta_M, \\ \text{i.e., } D^*(W_p)\eta \cdot \eta &> \theta_M |\eta|^2. \end{aligned}$$

(ii) The inequality (27) follows directly from (A1), (ii) of Lemma 1, and the identity

$$[D^*(W_p)]_{i,j} = \frac{1}{|Y|} \int_Y D(e_j + \nabla_y w_j) \cdot e_i \, dy$$

together with the Cauchy–Schwartz inequality. \square

Theorem 1 (Well-posedness of $P^k(\Omega)$). *Assume (A1)–(A4) hold and let $u^0 = g$. Then, there exist a sequence $(u^k, W^k)_{k \in \mathbb{N} \cup \{0\}} \subset \mathcal{U} \times L^\infty((0, T) \times \Omega; \mathcal{W}^2)$ such that, for each k , (u^{k+1}, W^k) uniquely solves the iterative scheme given by (8a)–(8g) in the sense of Definition 3.1. Moreover, we have $u^k, |\nabla u^k| \in L^\infty((0, T) \times \Omega)$ and satisfy*

$$\|u^k\|_{L^\infty((0, T) \times \Omega)} \leq \|g\|_{L^\infty(\Omega)} + T\|f\|_{L^\infty((0, T) \times \Omega)} \quad (41)$$

for all $k \in \mathbb{N}$.

Proof. We prove the existence of solutions via induction. By construction, we have $u^0 = g$ and the linear elliptic problems (8a)–(8c) have unique solutions $w_i^0(p, \cdot) \in \mathcal{W}$, where $p = G_i(u^0(t, x))$ for almost all $(t, x) \in (0, T) \times \Omega$ via Lemma 1 (i). Owing to Lemma 1 (ii), we have that $\|\nabla_y w_i(p, \cdot)\|_{L^2(\Omega)} \leq C$ uniformly in p . This implies $\|w_i(p, \cdot)\|_{\mathcal{W}} \leq C$ via the Poincaré–Wirtinger inequality and, as a consequence, it also holds that $W^0 = (w_1^0, w_2^0) \in L^\infty((0, T) \times \Omega; \mathcal{W}^2)$.

Let

$$m := \|g\|_{L^\infty(\Omega)} + T\|f\|_{L^\infty((0, T) \times \Omega)}$$

and set

$$M := \max_{r \in [-m, m]} \max_{i \in \{1, 2\}} |G_i(r)|.$$

M is well-defined as the functions G_i are continuous. Since $u^0 = g$, we also have $|G_i(u^0)| \leq M$. Using Lemma 3, we see that the dispersion tensor $D^*(W^0)$ satisfies

$$D^*(W^0)\eta \cdot \eta \geq \theta_M |\eta|^2$$

for all $\eta \in \mathbb{R}^2$ almost everywhere in $(0, T) \times \Omega$, where the constant $\theta_M > 0$ depends only on the choice of M .

The problem (8d)–(8f) is a standard linear parabolic problem. Benefiting of Assumptions (A1)–(A4) and of the uniform positivity of $D^*(W^0)$, the existence of a unique weak solution $u^1 \in \mathcal{U}$ to the problem (8d)–(8f) with $k = 0$ can be shown via standard Galerkin approximation arguments (see, e.g., [21, Chapter 7, Theorem 3]). The estimate

$$\|u^1\|_{L^\infty((0,T) \times \Omega)} \leq \|g\|_{L^\infty(\Omega)} + T\|f\|_{L^\infty((0,T) \times \Omega)}, \quad (42)$$

follows by an application of Duhamel's principle [39, Chapter 5], for details see [20, Lemma 10].

The solvability of the problem (8a)–(8f) for any $k \in \mathbb{N}$ follows by induction. Indeed, assume $u^k \in \mathcal{U}$ satisfies $u^k(0, \cdot) = g$ and

$$\|u^k\|_{L^\infty((0,T) \times \Omega)} \leq m, \quad (43)$$

it implies

$$G_i(u^k(t, x)) \in [-M, M], \quad i = 1, 2. \quad (44)$$

Then the existence of $W^k \in L^\infty((0, T) \times \Omega; \mathcal{W}^2)$ solving (8a)–(8c) follows by Lemma 1 in the same way as for W^0 . Relying on Lemma (3) and (44), we obtain that $D^*(W^k)$ is bounded and that for all $\eta \in \mathbb{R}^2$ it satisfies

$$D^*(W^k)\eta \cdot \eta > \theta_M |\eta|^2$$

almost everywhere in $(0, T) \times \Omega$, where $\theta_M > 0$ does not depend on k . Following the same arguments as before, we get the existence and uniqueness of $u^{k+1} \in \mathcal{U}$. The estimate

$$\|u^{k+1}\|_{L^\infty((0,T) \times \Omega)} \leq \|g\|_{L^\infty(\Omega)} + T\|f\|_{L^\infty((0,T) \times \Omega)},$$

follows similarly to (42). Now, using regularity result [28, Theorem 5.14], we obtain $u^k \in C^{2,1}((0, T) \times \Omega)$. □

3.3 Convergence of the iterative scheme

Now, we show that the sequence $(u^k, W^k)_{k \in \mathbb{N} \cup \{0\}}$ satisfies uniform energy estimates. These estimates are crucial in establishing the convergence of our scheme. We also present a proposition which will help us pass to the limit in the weak formulation.

Lemma 4. *Assume (A1)–(A4) hold and let $u^k \in \mathcal{U}$ be weak solution to the iterative scheme (8a)–(8f). Then, there exists a constant $C > 0$ independent of k such that*

$$\|u^k\|_{L^\infty((0,T); L^2(\Omega))} \leq C, \quad (45a)$$

$$\|\nabla u^k\|_{L^2((0,T); L^2(\Omega))} \leq C, \quad (45b)$$

$$\|\partial_t u^k\|_{L^2((0,T); H^{-1}(\Omega))} \leq C. \quad (45c)$$

Proof. Using (i) of Lemma 3 and (41), there exist $\theta_M > 0$ independent of k , depending on M such that

$$D^*(W^k)\eta \cdot \eta \geq \theta_M |\eta|^2$$

for all $\eta \in \mathbb{R}^2$. Estimates (45a)–(45c) then follow the arguments made in [21, Chapter 7, Theorem 2]. \square

Proposition 1. *Let $\xi_k, \psi_k, \xi, \psi \in L^2(\Omega)$ for all $k \in \mathbb{N}$. Assume*

$$\xi_k \rightarrow \xi \quad \text{strongly in} \quad L^2(\Omega), \quad (46)$$

$$\psi_k \rightharpoonup \psi \quad \text{weakly in} \quad L^2(\Omega) \quad (47)$$

and there exist a $C > 0$ independent of k , such that

$$\|\xi_k\|_{L^\infty(\Omega)} \leq C, \quad (48)$$

then for any $\phi \in L^2(\Omega)$, upto a subsequence we have

$$\lim_{k \rightarrow \infty} \int_{\Omega} \xi_k \psi_k \phi \, dx \rightarrow \int_{\Omega} \xi \psi \phi \, dx. \quad (49)$$

Proof. Using (46) and (47), we get

$$\xi_k \psi_k \rightharpoonup \xi \psi \quad \text{weakly in} \quad L^1(\Omega).$$

Hence for all $\phi \in C_c^\infty(\Omega)$, we have

$$\lim_{k \rightarrow \infty} \int_{\Omega} \xi_k \psi_k \phi \, dx \rightarrow \int_{\Omega} \xi \psi \phi \, dx. \quad (50)$$

Now, from (47) and (48), there exist a constant $C > 0$ independent of k , such that

$$\|\xi_k \psi_k\|_{L^2(\Omega)} \leq C. \quad (51)$$

So, by the weak compactness theorem, we get $\xi_k \psi_k$ weakly converges to some $h \in L^2(\Omega)$ in $L^2(\Omega)$. Now, combining with (50), we get $h = \xi \psi$ for a.e. $x \in \Omega$, which give us the required result (49). \square

Lemma 5. *Assume (A1)–(A4) hold and there exist $C > 0$ independent of k satisfying*

$$\|\nabla u^k\|_{L^\infty((0,T) \times \Omega)} \leq C. \quad (52)$$

Let $u^k \in \mathcal{U}$ be the weak solution to the iterative scheme (8a)–(8f), then u^k is a Cauchy sequence in $L^2(0, T; L^2(\Omega))$.

Proof. Let $k \in \mathbb{N}$, we have

$$\langle \partial_t u^{k+1}, \phi \rangle + \int_{\Omega} D^*(W^k) \nabla u^{k+1} \cdot \nabla \phi \, dx = \int_{\Omega} f \phi \, dx \quad (53)$$

$$\langle \partial_t u^k, \phi \rangle + \int_{\Omega} D^*(W^{k-1}) \nabla u^k \cdot \nabla \phi \, dx = \int_{\Omega} f \phi \, dx, \quad (54)$$

for all $\phi \in H_0^1(\Omega)$. Now, subtracting (54) from (53) and choosing $\phi = (u^{k+1} - u^k)$, we obtain

$$\frac{1}{2} \frac{d}{dt} \|u^{k+1} - u^k\|_{L^2(\Omega)}^2 + \int_{\Omega} (D^*(W^k) \nabla u^{k+1} - D^*(W^{k-1}) \nabla u^k) \cdot \nabla (u^{k+1} - u^k) dx = 0. \quad (55)$$

Adding and subtracting $\int_{\Omega} D^*(W^k) \nabla u^k \cdot \nabla (u^{k+1} - u^k) dx$, we get

$$\frac{1}{2} \frac{d}{dt} \|u^{k+1} - u^k\|_{L^2(\Omega)}^2 + \theta \|\nabla u^{k+1} - \nabla u^k\|_{L^2(\Omega)}^2 \leq \int_{\Omega} (D^*(W^{k-1}) - D^*(W^k)) \nabla u^k \cdot \nabla (u^{k+1} - u^k) dx. \quad (56)$$

Recalling that the functions G_i are locally Lipschitz (Assumption (A1)), i.e.,

$$|G_i(u^k) - G_i(u^{k-1})| \leq C|u^k - u^{k-1}|, \quad (57)$$

where $C > 0$ is independent of k since $|u^k|, |u^{k-1}| \leq m$. Using (57), we get

$$|D^*(W^{k-1}) - D^*(W^k)| \leq C|u^k - u^{k-1}|. \quad (58)$$

Using the aforementioned estimates and (52), we obtain

$$\frac{1}{2} \frac{d}{dt} \|u^{k+1} - u^k\|_{L^2(\Omega)}^2 + \theta \|\nabla u^{k+1} - \nabla u^k\|_{L^2(\Omega)}^2 \leq C \int_{\Omega} |u^k - u^{k-1}| |\nabla (u^{k+1} - u^k)| dx, \quad (59)$$

where $C > 0$ independent of k . Using Young's inequality and $u^{k+1}(0, \cdot) = u^k(0, \cdot)$, we get after integrating over time twice for any $t \in (0, T)$:

$$\|u^{k+1} - u^k\|_{L^2(0,t;\Omega)}^2 + \theta t \|\nabla (u^{k+1} - u^k)\|_{L^2((0,t);\Omega)}^2 \leq Ct \|u^k - u^{k-1}\|_{L^2(0,t;\Omega)}^2. \quad (60)$$

Choosing $t^* = \min\{2/C, T\}$ yields

$$\|u^{k+1} - u^k\|_{L^2(0,t^*;L^2(\Omega))} \leq \frac{1}{2} \|u^k - u^{k-1}\|_{L^2(0,t^*;L^2(\Omega))}. \quad (61)$$

Thus, we conclude u^k is Cauchy in $L^2(0, t^*; L^2(\Omega))$. By discretizing $(0, T)$ in small intervals $0 < t^* < 2t^* < \dots < T$, in a similar argument that leads to (61), we get u^k is Cauchy in $L^2(t^*, 2t^*; L^2(\Omega))$. Since we have $u^k \in C((0, T) \times \Omega)$, and using continuity argument we extend the result (61) in $(0, T) \times \Omega$, i.e., we get u^k is Cauchy in $L^2(0, T; L^2(\Omega))$ (for details see [32, Remark in Section 2] and [7, Section 7]). \square

Theorem 2 (Solvability of $P(\Omega)$). *Assume (A1)–(A4) hold and the constant C in (52) independent of k . Then, there exists a $u \in \mathcal{U}$ and a $W \in L^\infty((0, T) \times \Omega; \mathcal{W}^2)$ such that,*

$$u^k \rightarrow u \quad \text{strongly in } L^2((0, T) \times \Omega), \quad (62a)$$

$$D^*(W^k) \rightarrow D^*(W) \quad \text{strongly in } L^2((0, T) \times \Omega), \quad (62b)$$

and along a subsequence,

$$\nabla u^k \rightharpoonup \nabla u \quad \text{weakly in } L^2((0, T) \times \Omega), \quad (62c)$$

$$\partial_t u^k \rightharpoonup \partial_t u \quad \text{weakly in } L^2((0, T); H^{-1}(\Omega)). \quad (62d)$$

Moreover, (u, W) is a weak solution to the nonlinear parabolic-elliptic system (5a)–(5f) in the sense of Definition 2.1 and $u \in L^\infty((0, T) \times \Omega)$.

Proof. From Lemma 5, we get (62a). Using the weak compactness property (see [21, Appendix D, Theorem 3]) with the energy estimates (45b) and (45c), we get both (62c) and (62d). From (62a), it also follows that $u^k \rightarrow u$ pointwise almost everywhere in $(0, T) \times \Omega$. Hence, we obtain $u \in L^\infty((0, T) \times \Omega)$ and, more precisely, $|u| \leq m$. Via Lemma 1, we get the existence of the weak solution $w_i(p_i, \cdot) \in \mathcal{W}$ for (5d)–(5f) where $p_i = G_i(u(t, x))$, $i \in \{1, 2\}$, for almost all $(t, x) \in (0, T) \times \Omega$. This then extends to a function $W = (w_1, w_2) \in L^\infty((0, T) \times \Omega; \mathcal{W}^2)$ via Lemma 1 (ii).

Recalling (57), we can use the estimates (25) along with (62a) to show

$$\begin{aligned} \lim_{k \rightarrow \infty} \int_0^T \int_\Omega |[D^*(W^k) - D^*(W)]_{i,j}|^2 dx &= \lim_{k \rightarrow \infty} \int_0^T \int_\Omega |[\overline{D}(G_i(u^k)) - \overline{D}(G_i(u))]_{i,j}|^2 dx \\ &\leq C \lim_{k \rightarrow \infty} \int_0^T \int_\Omega |G_i(u^k) - G_i(u)|^2 dx \\ &\leq C \lim_{k \rightarrow \infty} \int_0^T \int_\Omega |u^k - u|^2 dx \\ &= 0. \end{aligned} \tag{63}$$

Using (62c) and (62b) together with Proposition 1, for any $\phi \in H_0^1(\Omega)$ we have

$$\lim_{k \rightarrow \infty} \int_\Omega D^*(W^k) \nabla u^{k+1} \cdot \nabla \phi dx = \int_\Omega D^*(W) \nabla u \cdot \nabla \phi dx. \tag{64}$$

Combining (62d) and (64) and then passing $k \rightarrow \infty$ in (9a), we see that u satisfies (7a). Hence, we have that (u, W) solves Problem $P(\Omega)$ in the sense of Definition 2.1. \square

We remark that the convergence of our scheme (8a)–(8f) does not guarantee the uniqueness of solutions to Problem $P(\Omega)$. However, under the assumption $\nabla u \in L^\infty((0, T) \times \Omega)$, uniqueness follows. Indeed, if u_1, u_2 solve Problem $P(\Omega)$, then by using the Lipschitz continuity of $D^*(W)$ (see Lemma (3)) and standard energy estimates for $u_1 - u_2$, we can conclude that $u_1 = u_2$ for almost every $(t, x) \in (0, T) \times \Omega$.

4 Numerical simulation

In this section, we demonstrate that the iteration scheme (8) can be used as a numerical method to approximate the solution of Problem $P(\Omega)$. Additionally, we use this numerical method to illustrate the impact of different microscopic geometries and to investigate how the effective dispersion tensor, D^* , governs the macroscopic behaviour of the system. To accomplish this, we make use of finite element method solvers in FEniCS [30, 26] with Lagrange polynomials of degree one as the basis elements for both the elliptic and parabolic problems. We begin by discretizing the macroscopic and microscopic domains. By first fixing an initial iteration u^0 , we can then solve the linear elliptic cell problems given by (8a)–(8c) in the microscopic domain for each point in the macroscopic domain. Please note that this step can be perfectly parallelized as each cell problem is independent. By calculating $D^*(W^k)$ given by (8g), we can then solve the linear parabolic problem (8d)–(8f), where we make use of an implicit Euler discretization to handle the time dependence. Then, using this numerical solution, we repeat these calculations for the next iteration. More concisely, given the numerical solution u^k , we calculate u^{k+1} by solving the linear system (8). We continue this

iteration method until a desired error tolerance between successive iterations (measured in the $L^2(0, T; L^2(\Omega))$ norm) is reached. We outline this approach in Algorithm 1.

To proceed with our investigation, we define two specific geometries (henceforth named geometry 1 and 2) which have different and interesting effects on the effective dispersion tensor. For geometry 1, we choose $Y = (0, 1)^2 \setminus \mathcal{B}_{0.25}((0.5, 0.5))$ where $\mathcal{B}_r((y_1, y_2))$ denotes the closed disk with radius r and center (y_1, y_2) (for a visualization, see the top row of Figure 2). For geometry 2, we let $Y = (0, 1)^2 \setminus (\mathcal{R}_1 \cup \mathcal{R}_2)$ with rectangles $\mathcal{R}_1 := [0.1, 0.9] \times [0.1, 0.2]$ and $\mathcal{R}_2 := [0.1, 0.9] \times [0.8, 0.9]$ (for a visualization, see the bottom row of Figure 2).

When choosing model ingredients, one difficulty is ensuring that the microscopic drift, $B(y)$, is both interesting, physically relevant, and satisfies the assumptions (A2) for each geometry. To accomplish this, we take the velocity field as the solution to the following Stokes problem:

Stokes problem for the drift velocity

$$-\mu\Delta B + \nabla p = F(y) \quad \text{in } Y, \quad (65a)$$

$$\operatorname{div} B = 0 \quad \text{in } Y, \quad (65b)$$

$$B = 0 \quad \text{on } \Gamma_N, \quad (65c)$$

$$y \mapsto B(y) \quad \text{is } Y\text{-periodic}, \quad (65d)$$

where Y is either geometry 1 or geometry 2. To ensure stability while solving (65), we use the Taylor-Hood elements in FEniCS, where second-order polynomials are used as basis function for the velocity field and first-order polynomials are used for the pressure. We refer the reader, for instance, to [10] for more information on the use of stable finite elements for the computation of Stokes flow.

For all simulations to follow, we choose $\mu = 0.01$ and

$$F : Y \rightarrow \mathbb{R}^2 \text{ given by } F(y) = (10 \sin(2\pi y_1) \sin(2\pi y_2), 10 \sin(2\pi y_1) \cos(2\pi y_2))$$

for $y = (y_1, y_2) \in Y$. The velocity vector $B(y) = (B_1(y), B_2(y))$ corresponding to geometry 1 and geometry 2 is shown in Figure 2.

4.1 Dispersion tensor

We now study the behaviour of the effective dispersion tensor with respect to the nonlinear drift interactions in both geometries. To begin with, we divide the interval $[-10, 10]$ into 101 equidistant nodes denoted p_i . We then solve the auxiliary cell problem given by (10a)-(10c) for each p_i . To enforce the fact that the cell solution has zero average, we use the Lagrange multiplier method in a similar manner as, for instance, in [22]. With the solutions to the cell problems, we compute the entries of the effective dispersion tensor using equation (6). These results are then interpolated and the components of D^* are plotted as a function of $p \in [-10, 10]$ in Figures 3 and 4.

Case 1: Fast diffusion We first consider the case where the microscopic diffusion is comparable in magnitude to the velocity field $B(y)$. To this end, we choose the diffusion matrix

$$D(y) = \begin{pmatrix} 2 + \sin(\pi y_1) \sin(\pi y_2) & 0 \\ 0 & 2 + \sin(\pi y_1) \end{pmatrix}, \quad y = (y_1, y_2) \in Y,$$

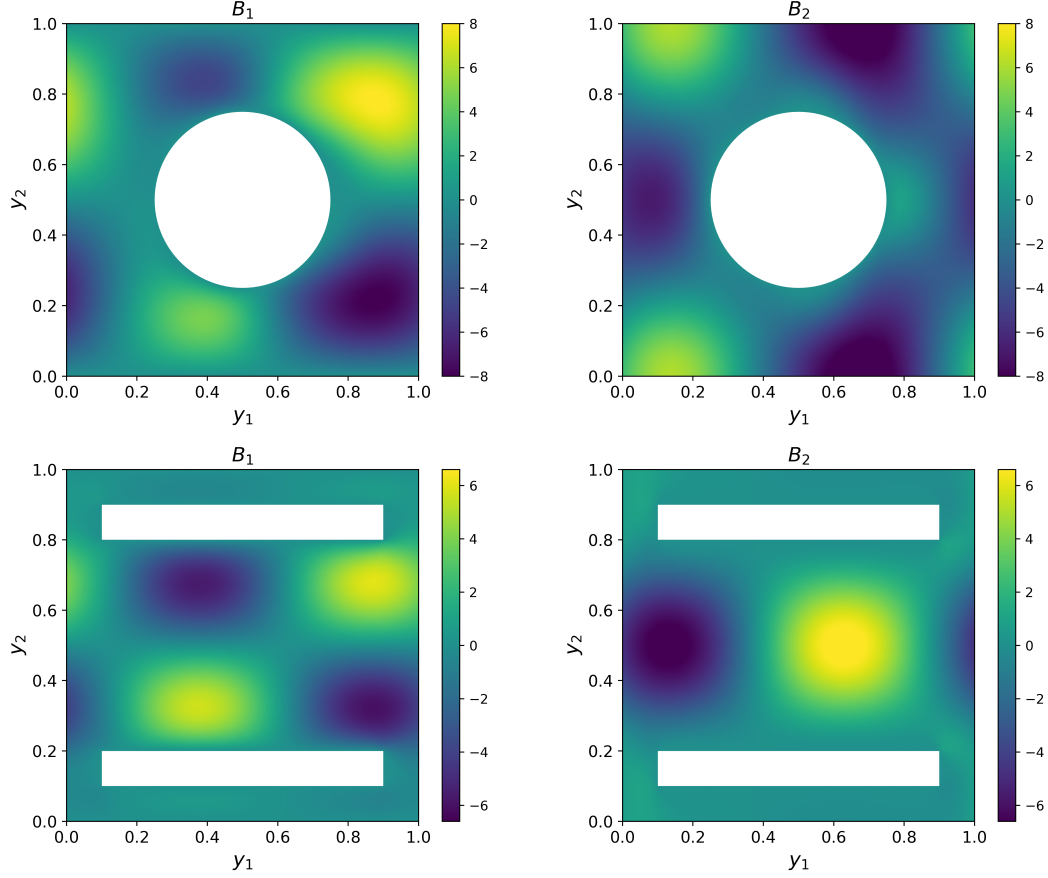


Figure 2: Top: solution to the Stokes problem, $B_1(y)$ (left) and $B_2(y)$ (right), in geometry 1. Bottom: solution to the Stokes problem, $B_1(y)$ (left) and $B_2(y)$ (right), in geometry 2.

which satisfies $1 \leq \det D(y) \leq 9$ everywhere in Y . Looking at Figure 3, we notice that the main diagonal entries D_{11}^* and D_{22}^* are symmetric with respect to the vertical axis while the off-diagonal entries D_{12}^* and D_{21}^* are symmetric about the origin. However, we note that the off-diagonal entries are close to 0 and have therefore only a small impact on the macroscopic dispersion. This is a consequence of both geometries being symmetric: in non-symmetric setups, e.g., angled rectangles or ellipses, the off-diagonal entries would play a bigger role. The particular case $p = 0$ corresponds to “no drift” and, in both geometries, it is the value with the slowest dispersion.

We can also see that while D_{11}^* and D_{22}^* are similar (both quantitatively and qualitatively) in the first geometry, they differ quite a bit in the second geometry. Focusing on geometry 2, the dispersion in y_1 direction appears to be much faster than in the y_2 direction as can be seen by D_{11}^* being almost twice as large as D_{22}^* . This is to be expected since the geometric setup with the two rectangles impedes vertical flows much more than lateral flows. More interestingly, D_{11}^* is close to constant in p while, on the other hand, D_{22}^* is much more dynamic with changes of up to 50% relative to the lowest value for $p = 0$. This shows that the drift interaction can play a large role in facilitating vertical flows for geometry 2.

Algorithm 1 Procedure to compute the weak solution to (8a)–(8f).

```

1: Discretize the space micro domain  $Y$  and macro domain  $\Omega$ 
2: Discretize the time domain  $[0, T]$  with step size  $\Delta t$ 
3: Solve the Stokes problem (65a)–(65d) to get  $B(y)$ 
4: Set initial iteration guess  $u^0$ 
5: Choose data  $f, D, G_i, g$ 
6: Set tolerance value  $\epsilon$ 
7: Set the maximum number of iterations,  $\text{Maxiter}$ .
8: Initialize iteration and time. i.e.  $iter = 0, t = 0$ 
9: while  $iter < \text{Maxiter}$  do
10:   Set  $u_{\text{old}} = g$ 
11:   Set  $u = [u_{\text{old}}]$ 
12:   for each time discrete node on time domain do
13:     for each node on macroscopic grid do
14:       Solve for  $(w_1, w_2)$  using  $(G_1(u_{\text{old}}), G_2(u_{\text{old}}))$ 
15:     end for
16:     Compute  $D^*$  from  $(w_1, w_2)$ 
17:     Solve for  $u_{\text{new}}$  using  $D^*$ 
18:     append  $u$  with  $u_{\text{new}}$ 
19:      $u_{\text{old}} \leftarrow u_{\text{new}}$ 
20:   end for
21:   if  $\|u - u^0\| < \epsilon$  then
22:     Stop
23:   end if
24:    $u^0 \leftarrow u$ 
25: end while

```

Case 2: Slow diffusion Now, we consider the slow diffusion case where the microscopic diffusion is small relative to the velocity field. We compute the components of the effective dispersion tensor and compare the results in both geometries in Figure 4. For this case, we choose the diffusion tensor to be

$$D(y) := \begin{pmatrix} 0.05 + \frac{1}{50} \sin(\pi y_1) \sin(\pi y_2) & 0 \\ 0 & 0.05 + \frac{1}{50} \sin(\pi y_1) \end{pmatrix}, \quad y = (y_1, y_2) \in Y,$$

which satisfies $0.009 \leq \det D(y) \leq 0.0049$ everywhere in Y . Comparing Figure 4 with Figure 3, we can observe very similar trends qualitatively although the values are, of course, much lower due to the slow diffusion. At first glance, it appears that there are cusps forming at the critical point $p = 0$ in D_{11}^* for geometry 1 and D_{22}^* for both geometries. However, a closer look shows that the transition is in fact smooth, see Figure 5. These observed “cusps” do however point to the fact that the slow diffusion case is much more volatile with respect to small changes close to the zero drift case $p = 0$ when compared to the fast diffusion case. Also, the relative changes in the dispersion values are higher than in the case of fast diffusion, e.g., in geometry 2 the value D_{22}^* experiences changes of more than 100% relative to the lowest value for $p = 0$.

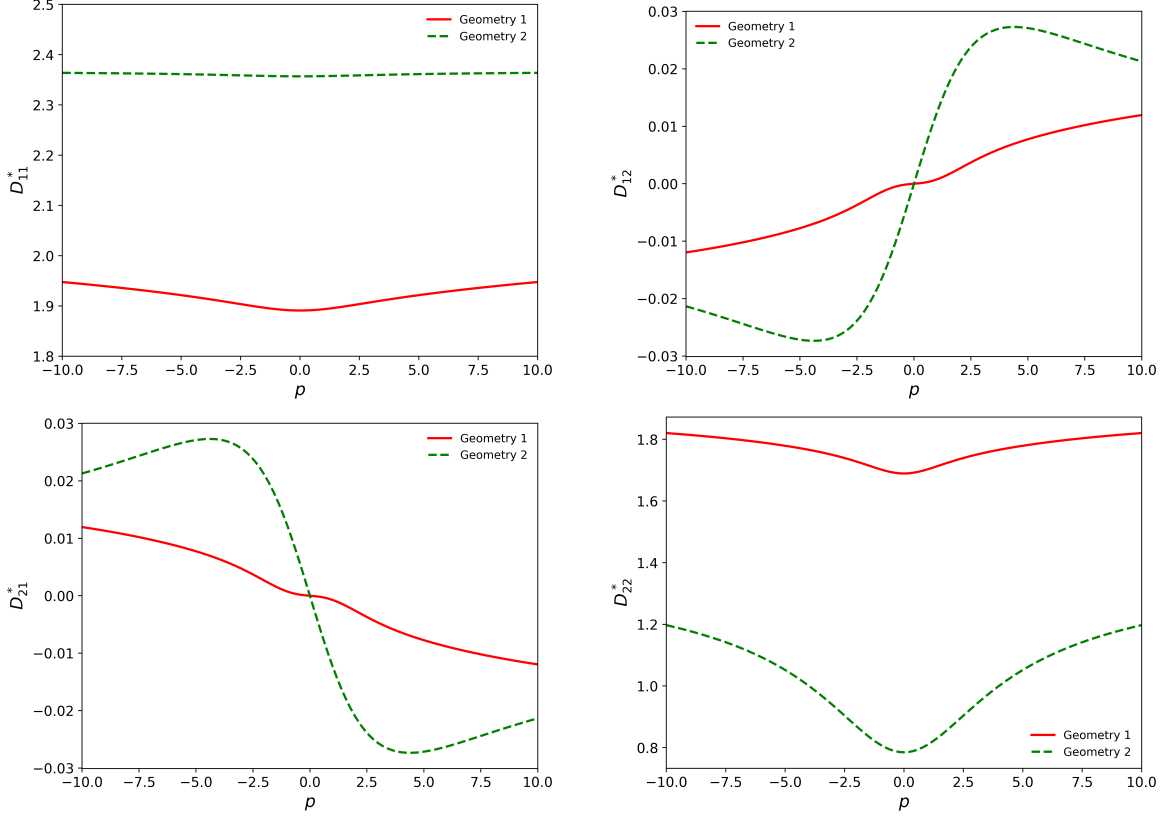


Figure 3: Comparison of the components of $D^*(W)$ for the fast diffusion case with both geometry 1 (solid red line) and geometry 2 (dashed green line). Here, we plot the components D_{11}^* (top left), D_{12}^* (top right), D_{21}^* (bottom left), and D_{22}^* (bottom right) as functions of the parameter p .

4.2 Macroscopic solution

The goal of this section is to illustrate how the behavior of the dispersion tensor presented above affects the solution to the macroscopic equation. In this section, we fix $\Omega = (0, 1) \times (0, 2)$ and the initial profile of concentration

$$g(x_1, x_2) = \begin{cases} \exp(-10((x_1 - 0.5)^2 + (x_2 - 0.5)^2)), & \text{if } (x_1, x_2) \in \mathcal{B}_{0.25}((0.5, 0.5)), \\ 0, & \text{otherwise.} \end{cases} \quad (66)$$

We also fix a constant source term $f : \Omega \rightarrow \mathbb{R}$ given by

$$f(x_1, x_2) = \begin{cases} 1000, & \text{if } (x_1, x_2) \in \mathcal{B}_{0.25}((0.5, 0.5)), \\ 0, & \text{otherwise.} \end{cases} \quad (67)$$

The iteration scheme requires an initial guess u^0 for which we choose $u^0(t, x) = g$. For the microscopic ingredients, we take the same diffusion matrix as in the fast diffusion case above for all simulations. The velocity field, $B(y)$, is treated in the same manner as before.

As explained previously, we iterate the FEniCS solvers until the maximum number of iterations is achieved or the error $e_k := \|u^{k+1} - u^k\|_{L^2(0, T, L^2(\Omega))} < \text{tol}$, where tol is a small tolerance value

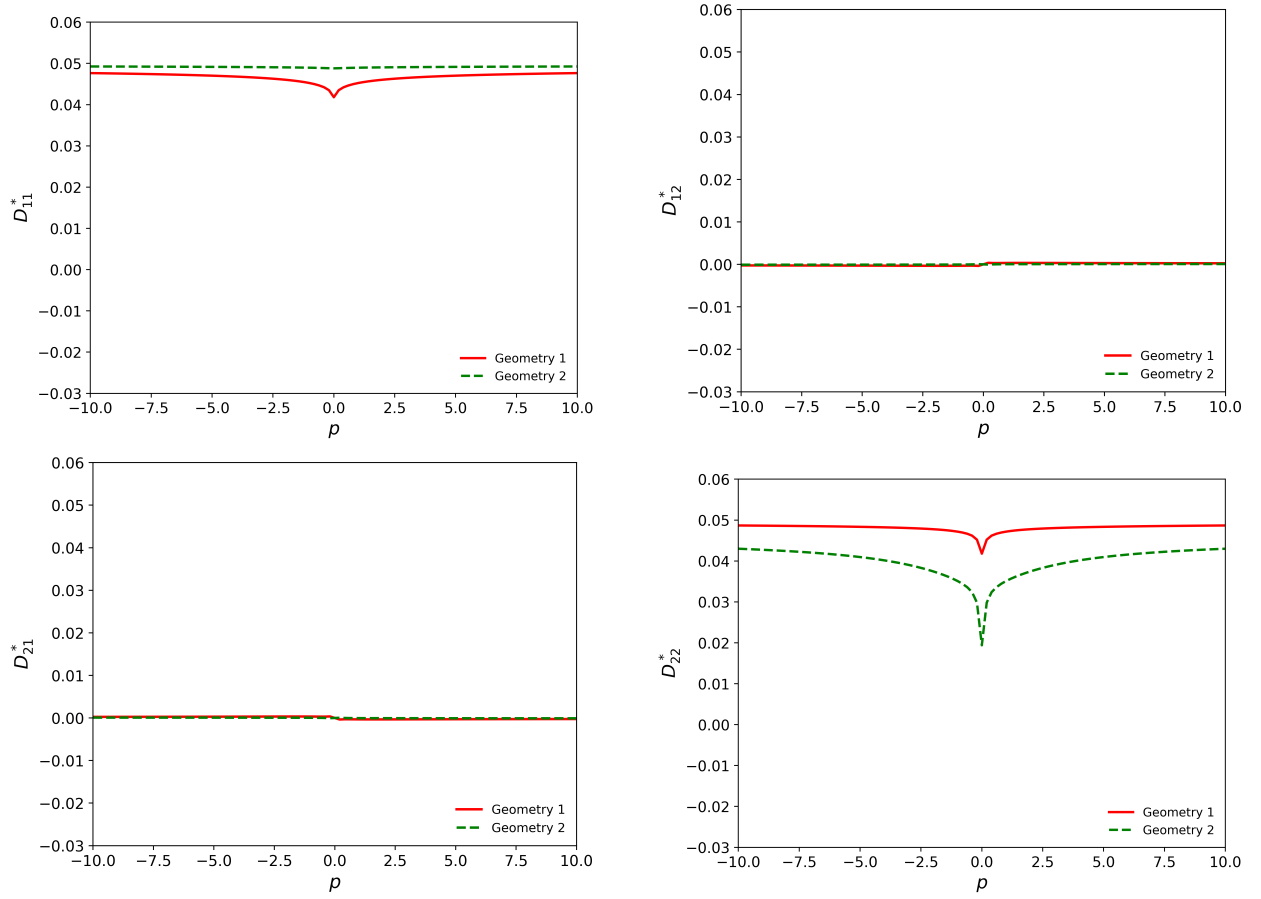


Figure 4: Comparison of the components of $D^*(W)$ for the slow diffusion case with both geometry 1 (solid red line) and geometry 2 (dashed green line). Here, we plot the components D_{11}^* (top left), D_{12}^* (top right), D_{21}^* (bottom left), and D_{22}^* (bottom right) as functions of the parameter p .

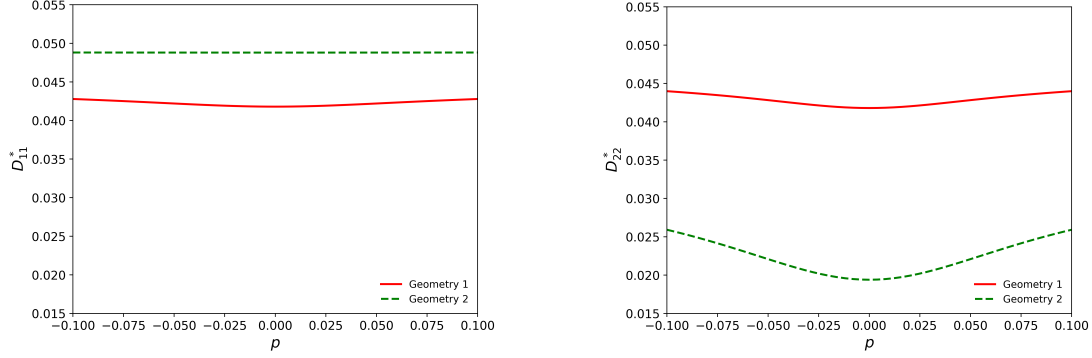


Figure 5: Comparison of two components of $D^*(W)$, D_{11}^* (left) and D_{22}^* (right), in the neighbourhood of $p = 0$ for the slow diffusion case.

prescribed *a priori* and $k \in \mathbb{N}$ is the iteration index. For all simulations, we choose $\text{tol} = 10^{-7}$ and use 50 space nodes in both directions in the macroscopic domain Ω . Additionally, we take $G_1(u) = G_2(u) = G(u)$ for these simulations.

Effect of the microscopic geometries In Figure 6, heat maps of the concentration profile u at time $T = 2$ with $G(u) = 1 - 2u$ using both microscopic geometries are displayed. Comparing the first and second plots in Figure 6, similar dispersive behavior of the concentration profiles is exhibited in both geometries. However, the concentration profile corresponding to geometry 1 disperses faster than that corresponding to geometry 2. This is expected as, due to the long horizontal rectangular obstacles in geometry 2, the flow is hindered in the vertical direction. The third plot in Figure 6 shows the difference between both solutions corresponding to the two different microscopic geometries. Looking at this difference, we observe that the concentration in the neighborhood of the point $(0.5, 0.5)$ is higher for geometry 2 than for geometry 1. To quantify this observed behavior, we calculate the total amount of the mass $M(t)$ of concentration u over time on the upper subdomain, $(0, 1) \times (1, 2)$, using the following formula:

$$M(t) := \int_1^2 \int_0^1 u(t, x_1, x_2) dx_1 dx_2. \quad (68)$$

We then plot the indicator $M(t)$ over time t for both choices of geometry in the left plot of Figure 8.

Effect of the nonlinear drift We now investigate how the nonlinear drift interactions affect the macroscopic dispersion. Here, all parameters are kept the same as in the previous numerical experiment, with the exception of the new nonlinearity $\tilde{G}(u) = 1/(0.0001 + |1 - 2u|)$ which we compare with the previous $G(u) = 1 - 2u$. The particular form of \tilde{G} is chosen to simulate the effect of high particle concentration impeding the flow. This can be seen by looking at Figure 3, where low values of $|G(u)|$ or $\tilde{G}(u)$ correspond to slightly slower dispersion than high values.

The macroscopic solution for both nonlinearities corresponding to geometry 2 at $T = 2$ is plotted in Figure 7. Similar to before, the concentration diffuses slower with the nonlinearity, $\tilde{G}(u)$, than with $G(u)$. Comparing the first and second plots in Figure 7, we observe that the solution profile is more concentrated around the source in the case of $\tilde{G}(u)$ (middle) than $G(u)$ (left). These effects

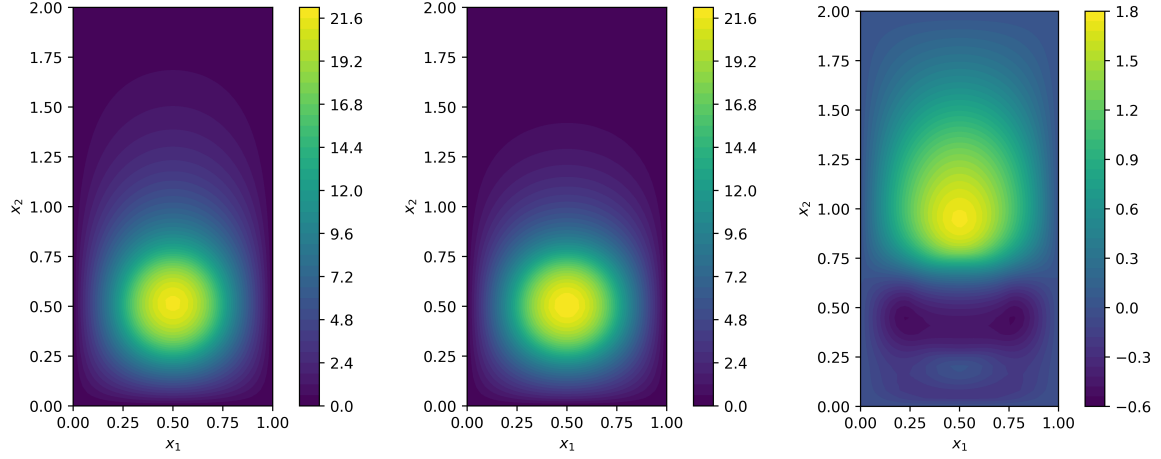


Figure 6: Macro-solution with $G(u) = 1 - 2u$ corresponding to microscopic geometry 1 (left), geometry 2 (middle), and the difference between these two solutions (right) at $T = 2$.

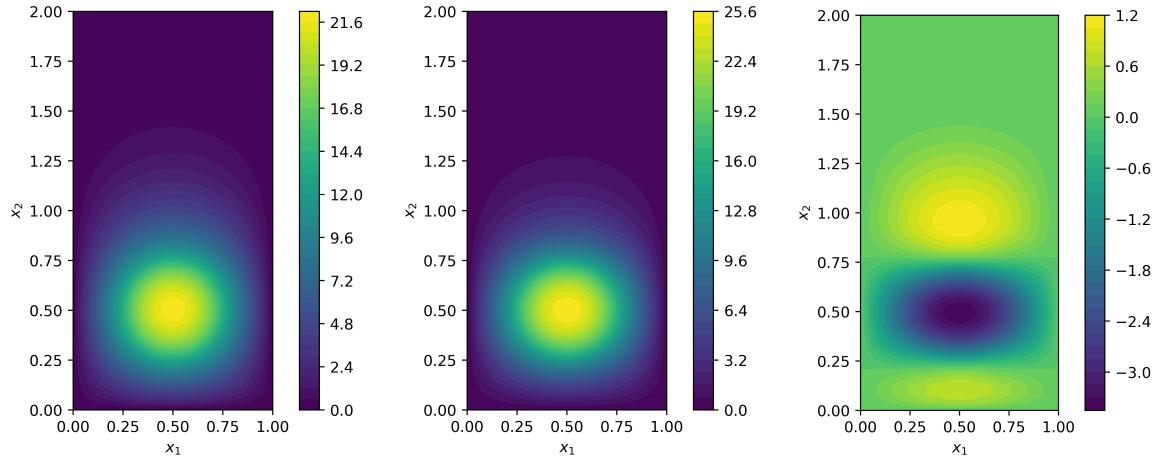


Figure 7: Macro-solution corresponding to geometry 2 with $G(u) = 1 - 2u$ (left), $\tilde{G}(u) = 1/(0.0001 + |1 - 2u|)$ (middle), and the difference between these two solutions (right) at $T = 2$.

can easily be seen in the right-most plot in Figure 7 where we calculate the difference between the concentration profiles. Similar observations can be made in the case of geometry 1, however, with these choices of ingredients, the difference is less drastic, and so, we omit these plots. As before, we examine the evolution of the mass in the upper subdomain, $M(t)$, and plot this in Figure 8 on the right.

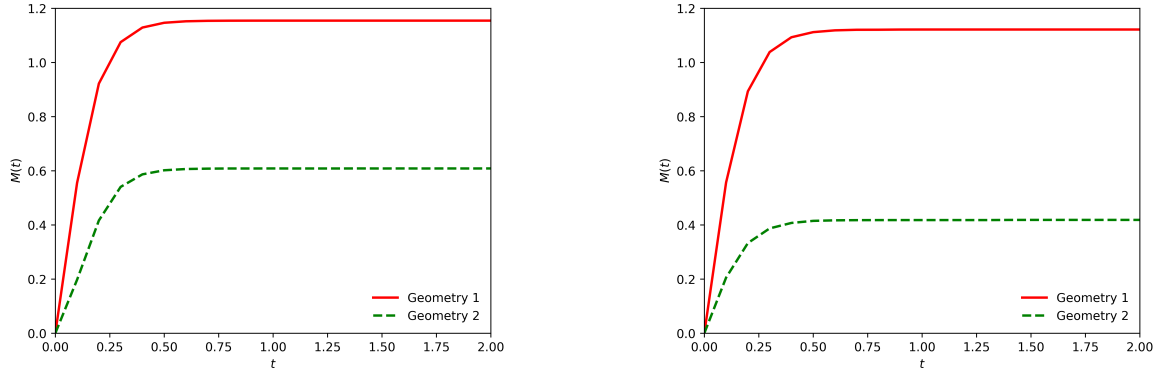


Figure 8: Comparison of mass $M(t)$ for geometry 1 (solid red line) and geometry 2 (dashed green line) with $G(u) = 1 - 2u$ (left) and $\tilde{G}(u) = 1/(0.0001 + |1 - 2u|)$ (right).

5 Conclusion and outlook

Understanding the effect microscopic fast drifts have on the structure of the macroscopic dispersion is generally a difficult task, even in the case of simple microstructures underlying a regular porous medium. We have shown in this paper that solutions to our model (Problem $P(\Omega)$) not only exist, but can also capture subtle two-scale effects of potential interest for applications. We will explore in follow-up works the numerical analysis of our setting as well as more numerical simulations of relevant practical case studies.

By constructing a convergent iterative scheme to Problem $P(\Omega)$, we have shown the existence of weak solutions, as well as the well-posedness of linear iterative approximations to the original two-scale system. We have implemented the constructed iterative scheme using finite element methods and numerically illustrated some potential effects the microscopic geometry and the drift coupling have on the macroscopic dispersion tensor. Such *a posteriori* effects can be seen either by examining the different profiles of the macroscopic solutions, or by following the time and space distribution of values in the entries of the effective dispersion tensor. We strongly believe that the working methodology proposed here can be used to approach a larger class of two-scale problems, covering among others the settings discussed, for instance, in [33, 5, 25, 41].

While the iteration scheme is a useful analytical tool, it is computationally expensive as the microscopic problem is solved for every time and space node in each iteration. However, given suitable assumptions about the choice of nonlinearity G , the dispersion tensor can be precomputed by solving the auxiliary problem (10a)–(10c) over a range of values for the parameter p in a similar way to the computations in Section 4.1. Additionally, this precomputing can be parallelized, as the microscopic cell problems are independent, and save a considerable amount of computation time. In light of this, we plan to study how this parallelization and precomputing technique affects the numerical results in terms of both the computation time and the order of accuracy. Of course, this requires us to additionally study the fully discrete error analysis of the Galerkin approximation (cf. e.g. [29, 36]) in order to determine the order of convergence in space and time.

Within the frame of this manuscript, we considered that the macroscopic problem is defined in a two-dimensional space since our motivation originated from a hydrodynamic limit performed for an interacting particles system (TASEP) posed in two dimensions. So, it is natural to take $\Omega \subset \mathbb{R}^2$. However, without much additional difficulty, we can extend our problem and the corresponding

results to dimension 3 and higher. The only notable change is that, if Problem $P(\Omega)$ is posed in $\Omega \times Y \subset \mathbb{R}^n \times \mathbb{R}^d$, then there will be d systems of nonlinear elliptic cell problems associated with the dispersion tensor. Additionally, the mathematical analysis work is not restricted to Dirichlet boundary conditions. Other choices of boundary conditions (e.g. homogeneous Neumann) are allowed as well. Furthermore, the macroscopic equation does not need to be scalar. A system of macroscopic equations coupled correctly with a family of elliptic cell problems can be handled as well in a similar fashion.

It is worth noting that we are currently unable to prove the uniqueness of solutions to Problem $P(\Omega)$ without assuming higher regularity. The main technical issue seems to be connected to the type of the nonlinearity arising in the structure of the dispersion tensor. Difficulties in proving the uniqueness of weak solutions to two-scale systems were also mentioned in [20]. There, the issue is a quite similar type of nonlinearity in the dispersion tensor. We are currently working to develop techniques tailored to prove uniqueness of solutions to this class of multiscale systems.

Acknowledgments

We thank H. Notsu (Kanazawa, Japan) and M. Alam (Mahindra University, India) for fruitful discussions during their visit to Karlstad. The work of V.R., S.N., and A.M. is partially supported by the Swedish Research Council's project "*Homogenization and dimension reduction of thin heterogeneous layers*" (grant nr. VR 2018-03648). The research activity of M.E. is funded by the European Union's Horizon 2022 research and innovation program under the Marie Skłodowska-Curie fellowship project *MATT* (project nr. 101061956). R.L. and A.M. are grateful to Carl Tryggers Stiftelse for their financial support via the grant CTS 21:1656.

References

- [1] A. Abdulle, E. Weinan, B. Engquist, and E. Vanden-Eijnden, *The heterogeneous multiscale method*, Acta Numerica **21** (2012), 1–87.
- [2] G. Allaire, *Homogenization and two scale convergence*, SIAM J. Math. Anal. **23** (1992), no. 6, 1482–1518.
- [3] G. Allaire and R. Brizzi, *A multiscale finite element method for numerical homogenization*, Multiscale Modeling & Simulation **4** (2005), no. 3, 790–812.
- [4] G. Allaire, R. Brizzi, A. Mikelić, and A. Piatnitski, *Two-scale expansion with drift approach to the Taylor dispersion for reactive transport through porous media*, Chemical Engineering Science **65** (2010), no. 7, 2292–2300.
- [5] G. Allaire and H. Hutridurga, *Upscaling nonlinear adsorption in periodic porous media – homogenization approach*, Applicable Analysis **95** (2016), no. 10, 2126–2161.
- [6] G. Allaire and A. Raphael, *Homogenization of a convection–diffusion model with reaction in a porous medium*, Comptes Rendus Mathématique **344** (2007), no. 8, 523–528.
- [7] Herbert Amann, *Ordinary differential equations: an introduction to nonlinear analysis*, vol. 13, Walter de Gruyter, 2011.

- [8] B. Amaziane, A. Bourgeat, and M. Jurak, *Effective macrodiffusion in solute transport through heterogeneous porous media*, Multiscale Modeling & Simulation **5** (2006), no. 1, 184–204.
- [9] R. Aris, *On the dispersion of a solute in a fluid flowing through a tube*, Proceedings of the Royal Society of London. Series A. Mathematical and Physical Sciences **235** (1956), no. 1200, 67–77.
- [10] D. N. Arnold, F. Brezzi, and M. Fortin, *A stable finite element for the Stokes equations*, Calcolo **21** (1984), no. 4, 337–344.
- [11] J.-L. Auriault, C. Moyne, and H. P. Amaral Souto, *On the asymmetry of the dispersion tensor in porous media*, Transport in Porous Media **85** (2010), no. 3, 771–783.
- [12] J. Bear, *Dynamics of Fluids in Porous Media*, Dover Publications, 1988.
- [13] J. Bear and L. G. Fel, *A phenomenological approach to modeling transport in porous media*, Transport in Porous Media **92** (2012), 649–665.
- [14] K. Bhattacharya, G. Friesecke, and R. D. James, *The mathematics of microstructure and the design of new materials*, Proceedings of the National Academy of Sciences **96** (1999), no. 15, 8332–8333.
- [15] C. Bringedal, L. von Wolff, and I. S. Pop, *Phase field modeling of precipitation and dissolution processes in porous media: Upscaling and numerical experiments*, Multiscale Modeling & Simulation **18** (2020), no. 2, 1076–1112.
- [16] C. Le Bris, F. Legoll, and F. Madiot, *Multiscale finite element methods for advection-dominated problems in perforated domains*, Multiscale Modeling & Simulation **17** (2019), no. 2, 773–825.
- [17] E. N. M. Cirillo, I. de Bonis, A. Muntean, and O. Richardson, *Upscaling the interplay between diffusion and polynomial drifts through a composite thin strip with periodic microstructure*, Meccanica **55** (2020), 2159–2178.
- [18] E. N. M. Cirillo, O. Krehel, A. Muntean, R. van Santen, and A. Sengar, *Residence time estimates for asymmetric simple exclusion dynamics on strips*, Physica A: Statistical Mechanics and its Applications **442** (2016), 436–457.
- [19] P. Donovan, Y. Chehreghanianzabi, M. Rathinam, and S. P. Zustiak, *Homogenization theory for the prediction of obstructed solute diffusivity in macromolecular solutions*, PLOS ONE **11** (2016), no. 1, 1–26.
- [20] M. Eden, C. Nikolopoulos, and A. Muntean, *A multiscale quasilinear system for colloids deposition in porous media: Weak solvability and numerical simulation of a near-clogging scenario*, Nonlinear Analysis: Real World Applications **63** (2022), 103408.
- [21] L. C. Evans, *Partial Differential Equations*, vol. 19, American Mathematical Society, 2010.
- [22] L. Formaggia, J.-F. Gerbeau, F. Nobile, and A. Quarteroni, *Numerical treatment of defective boundary conditions for the Navier–Stokes equations*, SIAM Journal on Numerical Analysis **40** (2002), no. 1, 376–401.

- [23] T. Goudon and F. Poupaud, *Homogenization of transport equations: A simple PDE approach to the Kubo formula*, Bulletin des Sciences Mathématiques **131** (2007), no. 1, 72–88.
- [24] P. Henning, M. Ohlberger, and B. Schweizer, *An adaptive multiscale finite element method*, Multiscale Modeling & Simulation **12** (2014), no. 3, 1078–1107.
- [25] E. Ijioma and A. Muntean, *Fast drift effects in the averaging of a filtration combustion system: A periodic homogenization approach*, Quarterly of Applied Mathematics **77** (2019), no. 1, 71–104.
- [26] H. P. Langtangen and A. Logg, *Solving PDEs in Python*, Springer International Publishing, 2016.
- [27] W. Li, L. Jiang, W. Jiang, Y. Wu, X. Guo, Z. Li, H. Yuan, and M. Luo, *Recent advances of boron nitride nanosheets in hydrogen storage application*, Journal of Materials Research and Technology **26** (2023), 2028–2042.
- [28] G. M. Lieberman, *Second Order Parabolic Differential Equations*, World scientific, 1996.
- [29] M. Lind, A. Muntean, and O. Richardson, *A semidiscrete Galerkin scheme for a coupled two-scale elliptic–parabolic system: well-posedness and convergence approximation rates*, BIT Numerical Mathematics **60** (2020), no. 4, 999–1031.
- [30] A. Logg, K.-A. Mardal, and G. Wells, *Automated Solution of Differential Equations by the Finite Element Method: The FEniCS Book*, vol. 84, Springer Science & Business Media, 2012.
- [31] D. Lukkassen, G. Nguetseng, and P. Wall, *Two-scale convergence*, International journal of pure and applied mathematics **2** (2002), no. 1, 35–86.
- [32] R. Lyons, E. N.M. Cirillo, and A. Muntean, *Phase separation and morphology formation in interacting ternary mixtures under evaporation – well-posedness and numerical simulation of a non-local evolution system*, arXiv preprint arXiv:2303.13981 (2023), 1–16.
- [33] E. Marušić-Paloka and A. L. Piatnitski, *Homogenization of a nonlinear convection-diffusion equation with rapidly oscillating coefficients and strong convection*, Journal of the London Mathematical Society **72** (2005), 391–409.
- [34] D.W. McLaughlin, G.C. Papanicolaou, and O.R. Pironneau, *Convection of microstructure and related problems*, SIAM Journal on Applied Mathematics **45** (1985), no. 5, 780–797.
- [35] A. Muntean and C. Nikolopoulos, *Colloidal transport in locally periodic evolving porous media—an upscaling exercise*, SIAM Journal on Applied Mathematics **80** (2020), no. 1, 448–475.
- [36] S. Nepal, Y. Wondmagegne, and A. Muntean, *Analysis of a fully discrete approximation to a moving-boundary problem describing rubber exposed to diffusants*, Applied Mathematics and Computation **442** (2023), 127733.
- [37] C. Nikolopoulos, M. Eden, and A. Muntean, *Multiscale simulation of colloids ingressing porous layers with evolving internal structure: A computational study*, GEM-International Journal on Geomathematics **14** (2023), no. 1, 1.

- [38] M. B. Olivares, C. Bringedal, and I. S. Pop, *A two-scale iterative scheme for a phase-field model for precipitation and dissolution in porous media*, Applied Mathematics and Computation **396** (2021), 125933.
- [39] R. Precup, *Linear and Semilinear Partial Differential Equations: An Introduction*, Berlin, Boston: De Gruyter, 2013.
- [40] V. Raveendran, E.N.M. Cirillo, I. de Bonis, and A. Muntean, *Scaling effects on the periodic homogenization of a reaction-diffusion-convection problem posed in homogeneous domains connected by a thin composite layer*, Quarterly of Applied Mathematics **80** (2022), 157–200.
- [41] V. Raveendran, E.N.M. Cirillo, and A. Muntean, *Upscaling of a reaction-diffusion-convection problem with exploding non-linear drift*, Quarterly of Applied Mathematics **80** (2022), 641–667.
- [42] V. Raveendran, I. de Bonis, E. N.M. Cirillo, and A. Muntean, *Homogenization of a reaction-diffusion problem with large nonlinear drift and Robin boundary data*, Quarterly of Applied Mathematics (2024), 1–39.
- [43] R.J. Schotting, H. Moser, and S.M. Hassanizadeh, *High-concentration-gradient dispersion in porous media: experiments, analysis and approximations*, Advances in Water Resources **22** (1999), no. 7, 665–680.
- [44] R. E. Showalter, *Distributed microstructure models of porous media*, Flow in Porous Media: Proceedings of the Oberwolfach Conference, June 21–27, 1992, Springer, 1993, pp. 155–163.
- [45] G. I. Taylor, *Conditions under which dispersion of a solute in a stream of solvent can be used to measure molecular diffusion*, Proceedings of the Royal Society of London. Series A. Mathematical and Physical Sciences **225** (1954), no. 1163, 473–477.
- [46] D. Wiedemann and M. A. Peter, *Homogenisation of local colloid evolution induced by reaction and diffusion*, Nonlinear Analysis **227** (2023), 113168.
- [47] B. D. Wood, F. Cherblanc, M. Quintard, and S. Whitaker, *Volume averaging for determining the effective dispersion tensor: Closure using periodic unit cells and comparison with ensemble averaging*, Water Resources Research **39** (2003), no. 8.